# Fiducial Points-supported Object Pose Tracking on RGB Images via Particle Filtering with Heuristic Optimization

Mateusz Majcher and Bogdan Kwolek

*AGH University of Science and Technology*
*30 Mickiewicza, 30-059 Krakow, Poland*
*{majcher, bkw}@agh.edu.pl*

Keywords:     6D object pose, object segmentation, pose tracking.

Abstract:      We present an algorithm for tracking 6D pose of the object in a sequence of RGB images. The images are acquired by a calibrated camera. A particle filter is utilized to estimate the posterior probability distribution of the object poses. The probabilistic observation model is built on the projected 3D model onto image and then matching the rendered object with the segmented object. It is determined using object silhouette and distance transform-based edge scores. A hypothesis about 6D object pose that is calculated on the basis of object keypoints and the PnP algorithm is included in the probability distribution. A k-means++ algorithm is then executed on multi-modal probability distribution to determine modes. A multi-swarm particle swarm optimization is executed afterwards to find finest modes in the probability distribution together with the best pose. The object of interest is segmented by an U-Net neural network. Eight fiducial points of the object are determined by a neural network. A data generator employing 3D object models has been developed to synthesize photorealistic images with ground-truth data for training neural networks both for object segmentation and estimation of keypoints. The 6D object pose tracker has been evaluated both on synthetic and real images. We demonstrate experimentally that object pose hypotheses calculated on the basis of fiducial points and the PnP algorithm lead to considerable improvements in tracking accuracy.

## 1  INTRODUCTION

It is expected that in the near future, robots will perform routine tasks that they are not able to perform today. Estimating the 6-DoF pose (3D rotations + 3D translations) of an object with respect to the camera is crucial to realize such tasks. Delivering robust estimates of the object pose on the basis of RGB images is a difficult problem. The discussed task has many important aspects that should be resolved to achieve robust object grasping, including object classification, object detection, object tracking, object segmentation and finally, estimation of the 6D object pose. A lot of successful researches have been done in these directions (He et al., 2017; Deng et al., 2019).

The most simple way for camera pose estimation consists in using squared markers, for instance ArUco markers (Garrido-Jurado et al., 2014). However, having on regard that the marker detection is based on high contrast edges in the image as well as overall high intensity contrast between the black and white areas of the marker, such methods are prone to motion blur caused by fast marker or camera movement,

mainly due to unsharp or blurred edges (Marchand et al., 2016). In Perspective-n-Point (PnP) algorithm (Fischler and Bolles, 1981) the pose of a calibrated camera is estimated on the basis of a set of 3D points in the world and their corresponding 2D projections in the image. However, the correspondence-based approaches require rich texture features. They calculate the pose using the PnP and recovered 2D-3D correspondences, often in a RANSAC (Fischler and Bolles, 1981) framework to support outlier rejection. While PnP algorithms are usually robust when the object is well textured, they can fail when it is featureless or when in the scene there are multiple objects occluding each other.

A large variety of object pose estimation approaches relying on natural point features have been proposed in the past, e.g. (Lepetit et al., 2004; Vidal et al., 2018), to enumerate only some of them. In general, features can either encode image properties or be a result of learning.

Recently, great progress has been made on estimating 6D object pose from the 2D image via deep learning-based architectures. A first attempt to use

a convolutional neural network (CNN) for direct regression of 6DoF object poses was PoseCNN (Xiang et al., 2018). For example, in (Kehl et al., 2017) the authors treat the pose estimation as a classification problem and train neural networks to classify the image features into a discretized pose space. In general, two main CNN-based approaches to 6D pose object pose estimation have emerged: either regressing the 6D object pose from the image directly (Xiang et al., 2018) or predicting 2D key-point locations in the image (Rad and Lepetit, 2017), from which the object pose can be determined by the PnP algorithm. In (Rad and Lepetit, 2017) the whole process is divided into two stages. In the first stage the authors determine the centres of objects of interest, and afterwards they use deep neural networks to determine the rotation of the object. In (Peng et al., 2019), a Pixel-wise Voting Network (PVNet) to regress pixel-wise unit vectors pointing to the keypoints and then using these vectors to vote for keypoint locations via RANSAC has been proposed. Instead of directly regressing image coordinates of keypoints, their method predicts unit vectors that represent directions from each pixel of the object towards the keypoints, then these directions vote for the keypoints locations based on RANSAC.

There are several publicly available datasets for benchmarking the performance of algorithms for 6D object pose estimation, including OccludedLinemod (Brachmann et al., 2014), YCB-Video (Xiang et al., 2018). However, the current datasets do not focus on 6D object tracking using RGB image sequences. They are mainly designed for single-frame based pose estimation. The data do not contain distortions (e.g. motion blur caused by fast object motions) and freestyle object motions, which are common in real-world scenarios.

In this work we investigate the problem of 6-DOF object pose estimation and tracking on RGB images acquired from a calibrated camera. U-Net neural network is used to segment the object of interest. The segmented object is then fed to a neural network estimating the 2D position of eight fiducial points of the object. Afterwards, the 6D object pose is estimated using the PnP algorithm and then used as a pose hypothesis during the pose inference. A particle filter (PF) combined with a particle swarm optimization (PSO) is utilized to estimate the posterior probability distribution of the object poses as well as the best pose. The observation model and objective function are calculated on the basis of the projected 3D model onto images and then matching the rendered object with the segmented object. It is determined using object silhouette and distance transform-based edge scores. A hypothesis about 6D object pose that is cal-culated on the basis of eight fiducial keypoints and the PnP algorithm is included in the probability distribution of the object poses. A k-means++ algorithm is then executed on multi-modal probability distribution. A particle swarm optimization is executed afterwards to find the modes in the probability distribution. The fiducial points of the object are determined by a neural network. A data generator employing 3D object models has been developed to synthesize photorealistic images with ground-truth data for training neural networks both for object segmentation and estimation of keypoints. The 6D object pose tracker has been evaluated both on synthetic and real images with six objects. In order to capture real images each of six objects has been placed on top of an electric turntable and then captured from four camera elevations. We demonstrate experimentally that object hypotheses calculated on the basis of fiducial points and the PnP algorithm permit achieving considerable improvements in tracking accuracies.

## 2 OBJECT SEGMENTATION

The architecture of neural network for object segmentation has been based on the U-Net (Ronneberger et al., 2015). The architecture of U-Net resembles the letter U, which is why it is called so. In such networks we can distinguish a contracting path (encoding) path and an expansive (decoding) path. In the contraction path, each block consists of a series of $3\times3$ convolution layers followed by a $2\times2$ max pooling, where the number of cores after each block doubles. A characteristic feature of the U-Net architecture is the expansive path, which also, by analogy with the contracting path, consists of several expansion blocks. In this path, the $2\times2$ max pooling is replaced by a $2\times2$ upsampling layer. Each step in the expanding path consists of the upsampling operation followed by a $2\times2$ convolution, combining with an appropriately cropped property map, and this is completed by two $3\times3$ convolutions, followed by ReLU. Skip connections used in U-Net directly connects the feature maps between encoder and decoder. The neural network was trained on RGB images. To reduce the training time, prevent overfitting and to increase performance of the U-Net we added Batch Normalization (BN) (Ioffe and Szegedy, 2015) after each `Conv2D`. As it improves gradient flow through the network, it reduces dependence on initialization and higher learning rates are achieved. Data augmentation has also been applied during the network training. The pixelwise cross-entropy has been used as the loss function.

# 3  6D OBJECT POSE ESTIMATION

The 6D pose is estimated using a CNN, which delivers 2D locations of eight fiducial points of the object. The 2D locations of such points are then fed to a PnP algorithm, that delivers the 6D pose of the object. A segmented image of size $128\times128$ pixels is delivered from the U-Net CNN to the fiducial CNN as input, which determines 2D locations of eight keypoints. Figure 1 shows a schematic architecture of fiducial CNN. The network architecture has been designed in such a way as to obtain, on the one hand, sufficient precision in the estimation of the position of keypoints in the images, and on the other hand, to avoid introducing unnecessary delays in the estimation of the position of the points during the pose tracking. The first part consists of 2 blocks, where each one contains convolutional layer with $3\times3$ kernels, followed by max-pooling with kernel of size $2\times2$, respectively. The layers are completed by the batch normalization and ReLU activation function. The next part consists of 3 consecutive convolutional layers with $3\times3$ kernels followed by max-pooling with kernel of size $2\times2$. In the MLP part, in the first two layers there are 512 neurons in each layer, and in the last there are 16 neurons that deliver the positions of 8 pairs of keypoints of the object. The loss function was mean absolute error (MAE). This network is a result of several experiments aiming at finding possibly small neural network, while still achieving pose estimates with accuracy sufficient for object grasping. For each object a separate network has been trained. Given class information determined by segmentation networks like mask-RCNN (He et al., 2017), the network for pose estimation can be selected automatically.



Figure 1: Neural network for estimation of fiducial points.

The discussed neural network requires input images of size $128 \times 128$ with the segmented object of interest. During pose tracking a ROI containing the object can be extracted easily using information from the previous frame and then scaled to desirable size.

## 3.1  PF-PSO with PnP-based Hypotheses

The algorithm extends the algorithm for 6D pose tracking (Majcher and Kwolek, 2020), which combines particle filtering and particle swarm optimization as well as effectively utilizes the k-means++

(Arthur and Vassilvitskii, 2007) for better dealing with multimodal distributions. Given the particle set representing the posterior probability distribution in the previous frame, the particles are propagated according to a probabilistic motion model, the pose likelihoods on the basis of probabilistic observation model are calculated, and afterwards the particle weights are determined and a resampling is executed, see also Fig. 2, as in ordinary particle filters. A particle with a small weight is replaced in such a resampled particle set by a particle with pose determined on the basis of keypoints and the PnP algorithm, see line #2 in below pseudo-code. Next, samples are clustered using k-means++ algorithm (Arthur and Vassilvitskii, 2007), which applies a sequentially random selection strategy according to a squared distance from the closest center already selected. Afterwards, a two-swarm PSO is executed to find the modes in the probability distribution. The number of the iterations executed by the PSO is set to three. Next, ten best particles are selected to form a sub-swarm, see lines #6-7 in below pseudo-code. Twenty iterations are executed by such a sub-swarm to find better particle positions. The best global position returned by the discussed sub-swarm is used in visualization of the best pose. Finally, an estimate of the probability distribution is calculated by replacing the particle positions determined by the PF with corresponding particle positions, which were selected to represent the modes in the probability distribution, see lines #6-7, and particles refined by the sub-swarm, see line #9. The initial probability distribution is updated by ten particles with better positions found by the PSO algorithms and ten particles with better positions found by the sub-swarm, see lines #9-11. The probabilistic motion model, observation model and objective function in the PSO are the same as in (Majcher and Kwolek, 2020).

```
1    function select(n_best, X)
2        X_sorted = quicksort(X) using f()
3    return X_sorted[1...n_best]
```

```
1    X_t = PF(X_{t-1})
2    x_t^{PnP} = PnP(), replace worst x ∈ X_t with x_t^{PnP}
3    X_t^{c1}, X_t^{c2} = k-means++(X_t)
4    ~, X_t^{c1} = PSO(X_t^{c1}, 3)
5    ~, X_t^{c2} = PSO(X_t^{c2}, 3)
6    X_t^{c1_best} = select(5, X_t^{c1})
7    X_t^{c2_best} = select(5, X_t^{c2})
8    X_t^{best} = X_t^{c1_best} ⋃ X_t^{c2_best}
9    g_best, X_t^{best} = PSO(X_t^{best}, 20)
10   substitute 5 x ∈ X_t with corresp. x ∈ X_t^{c1_best}
11   substitute 5 x ∈ X_t with corresp. x ∈ X_t^{c2_best}
13   substitute 10 x ∈ X_t with corresp. x ∈ X_t^{best}
14   return g_best, X_t
```
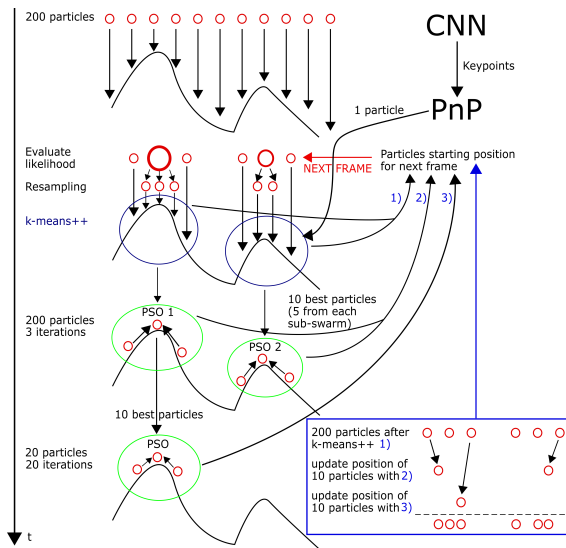
Figure 2: PF-PSO supported with pose hypotheses, which are determined on the basis of keypoints and the PnP.

## 4 DATASET

To evaluate and compare pose estimation algorithms, a number of benchmark datasets have been proposed, including: Linemod (Hinterstoisser et al., 2013), Linemod-Occluded (Brachmann et al., 2014), T-LESS (Hodan et al., 2017), YCB-Video (Xiang et al., 2018), HomebrewedDB (Kaskman et al., 2019). The datasets are mainly designed for single-frame based pose estimation. They do not contain distortions (e.g. motion blur caused by fast object motions) and free-style object motions, which are important for experiments and performance evaluation in real-world scenarios. A recently proposed dataset (Wu et al., 2017) has been designed for pose tracking and addresses issues mentioned above. In particular, it contains binary masks for real objects. However, this dataset has not been designed for algorithms based on deep learning. For instance, it does not contain keypoints data and therefore neural networks for 6D pose estimation on the basis of keypoints (Zhao et al., 2018) can not be trained. Moreover, in 3D object sub-dataset only objects generated by a 3D printer are available. This means that it does not permit a comparison of results obtained for frequently used objects in popular datasets, like power drill from YCB-Video dataset. This motivated us to utilize an extended dataset for 6D object tracking (Lopatin and Kwolek, 2020).

Our dataset contains six objects: drill, multimeter, electrical extension, duck, frog and piggy. The extension, duck, frog, and piggy are texture-less or almost texture-less. 3D models of the objects were prepared manually using Blender, which is a 3D computer graphics software toolset (Blender Online Community, 2020). The diameter of the first object is 228 mm and the 3D model consists 417777 vertices, the diameter of the second object is 138 mm and 3D model contains 119273 vertices, the diameter of third object is 103 mm and 3D model contains 216233 vertices, the diameter of the fourth object is 117 mm and 3D model contains 140148 vertices, the diameter of the fifth object is 108 mm and 3D model contains 135072 vertices, and the diameter of the sixth object is equal to 116 mm and its 3D model consists 132620 vertices. The 3D models of the objects have been designed using 2.81 software version of Blender. Figure 3 depicts rendered images, which were obtained on the basis of our 3D models. The images were rendered using Python scripts (Lopatin and Kwolek, 2020) with Blender's engine support. As we can observe, our 3D models permit photo-realistic rendering of the objects in the requested poses.



(a) Duck  (b) Piggy  (c) Frog

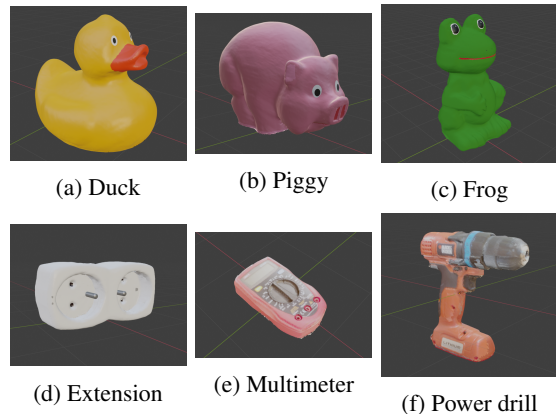(d) Extension  (e) Multimeter  (f) Power drill

Figure 3: Samples of real images.

We generated images for training neural networks both for object segmentation/detection and tracking. For object detection and object segmentation the object masks are stored both in images with binary masks as well as .json files, which are compatible with coco data format (Lin et al., 2014). The binary masks are stored in .png images with alpha (transparency) channel. The .jsn files contain also 3D positions of eight fiducial points. Even if a fiducial point is occluded, it is generated on the image. Thus, the number of fiducial points is constant despite occlusions or self-occlusions. This means that neural networks like mask-RCNN can be trained easily not only for object detection or segmentation, but also after small

modification of the code for estimation of position of fiducial points on the RGB images. The information about 6D pose of the objects is also stored in the .json files. It is worth noting that popular datasets for 6D object pose estimation do not contain data on object keypoints, i.e. fiducial points of the objects, and usually contain only information on the 3D positions of the rectangular corners describing the object of interest, and thus automatically determined from the position of the camera or ArUco markers. The tracking sub-dataset contains images with three types of motion: (i) object moves from left to right and then from right to left, (ii) object moves and simultaneously rotates from $0 \ldots 180°$ and then makes full rotation and (iii) object moves, simultaneously rotates and changes distance to the camera.

In addition to the synthetic data mentioned above, the dataset contains also real data. The camera has been calibrated using the OpenCV library (Bradski and Kaehler, 2013). The ground truths of the object poses have been determined using measurements provided by a turntable. Each object has been observed from four different camera views, see Fig. 4. The objects were rotated in range $0° \ldots 360°$. During object rotation, every ten degrees an image has been acquired with corresponding rotation angle. This means that for each object the number of images acquired in such a way is equal to 144.
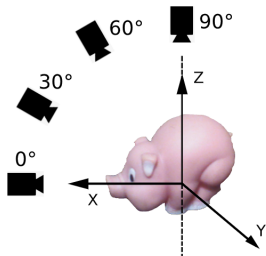


Figure 4: Camera setting.

For training the object segmentation models the objects were rotated and observed by the camera from different views. For each considered object, 150 images with manual delineations of the objects (Lopatin and Kwolek, 2020) were prepared and stored in the dataset. Additionally, 2D locations of fiducial points are stored in corresponding files. This subset consisting of real RGB images with the corresponding ground truth data can be employed for training as well as evaluation of neural networks for 6D object pose estimation and tracking. The data are stored in the format that is identical with data format utilized in the synthetic subset.

# 5 EXPERIMENTAL RESULTS

At the beginning of this Section we discuss evaluation metric for 6D pose estimation, Afterwards, we present experimental results.

## 5.1 Evaluation Metric for 6D Pose Estimation

We evaluated the quality of 6-DoF object pose estimation using ADD score (Average Distance of Model Points) (Hinterstoisser et al., 2013). ADD is defined as average Euclidean distance between model vertices transformed using the estimated pose and the ground truth pose. This means that it expresses the average distance between the 3D points transformed using the estimated pose and those obtained with the ground-truth one. It is defined as follows:

$$ADD = \text{avg}_{x \in M} ||(Rx + t) - (\hat{R}x + \hat{t})||_2 \qquad (1)$$

where $M$ is a set of 3D object model points, $t$ and $R$ are the translation and rotation of a ground truth transformation, respectively, whereas $\hat{t}$ and $\hat{R}$ correspond to those of the estimated transformation. This means that it expresses the average distance between the 3D points transformed using the estimated pose and those obtained with the ground-truth one. The pose is considered to be correct if average distance $e$ is less than $k_e d$, where $d$ is the diameter (i.e., the largest distance between vertices) of $M$ and $k_e$ is a pre-defined threshold (normally it is set to ten percent).

We determined also the rotation error on the basis of the following formula:

$$err_{\text{rot}} = \arccos((Tr(\hat{R}R^{-1}) - 1)/2) \qquad (2)$$

where $Tr$ stands for matrix trace, $\hat{R}$ and $R$ denote rotation matrixes corresponding to ground-truth and estimated poses, respectively.

## 5.2 Evaluation of Pose Tracking

At the beginning we evaluated a basic version of the algorithm (Majcher and Kwolek, 2020), i.e. without PnP-based hypotheses to support PF-PSO on freely available OPT benchmark dataset (Wu et al., 2017), which has been recorded for tracking of 6D pose of the objects. In discussed dataset the image sequences were recorded under various lighting conditions, different motion patterns and speeds using a programmable robotic arm. Table 1 presents the tracking scores achieved in 6D pose tracking of House and Ironman objects in FreeMotion scenario.

Table 1: Tracking scores [%] achieved by basic version of our algorithm in tracking 6D pose of House and Ironman in FreeMotion scenario.

| tracking score [%] | House | Ironman |
|---|---|---|
| Behind, ADD 10% | 88 | 41 |
| Behind, ADD 20% | 100 | 66 |
| Left, ADD 10% | 82 | 32 |
| Left, ADD 20% | 98 | 61 |
| Right, ADD 10% | 60 | 51 |
| Right, ADD 20% | 86 | 83 |
| Front, ADD 10% | 56 | 28 |
| Front, ADD 20% | 89 | 51 |
| Average, ADD 10% | 72 | 38 |
| Average, ADD 20% | 93 | 65 |

Table 2 contains AUC scores achieved by recent methods in 6D pose tracking of House and Ironman objects in FreeMotion scenario. As we can observe, our algorithm in basic version achieves better results in comparison to results achieved by PWP3D, UDP and ElasticFusion. In comparison to results in (Bugaev et al., 2018) it achieves slightly worse results on House object and worse results on the Ironman.

Table 2: AUC scores achieved in tracking 6D pose of House and Ironman in FreeMotion scenario, compared to results achieved by recent methods.

| AUC score [%] | House | Ironman |
|---|---|---|
| (Prisacariu and Reid, 2012) | 3.58 | 3.92 |
| (Brachmann et al., 2016) | 6.04 | 5.16 |
| (Whelan et al., 2016) | 2.83 | 1.75 |
| (Bugaev et al., 2018) | 14.48 | 14.71 |
| Our method | 12.12 | 5.16 |

Since the OPT benchmark dataset does not contain enough data to train and evaluate of neural networks for fiducial point estimation, we conducted experiments on our dataset. For evaluation of 6D pose tracking we selected the sequences #2 in which the objects move from left to right, simultaneously make rotations from 0 to 180°, and after reaching the right side of the image, the objects move back from right to left, simultaneously make full rotation about axis. The training of neural networks both for object segmentation/detection and 6D pose estimation was done on synthetic images only. Table 3 presents experimental results that were obtained by our algorithm.

Table 4 compares results achieved by our algorithm with and without the PnP algorithm. As we can observe, thanks to employing in the PF-PSO algorithm an additional information about object poses, far better tracking scores can be achieved for all considered objects.

Figure 5 depicts ADD scores over time that were obtained by the PF-PSO with neural network estimating position of fiducial points and the PnP algorithm. As we can observe, slightly bigger errors were

Table 3: Tracking scores [%] achieved by our algorithm in tracking 6D pose of objects.

| ⊲,ADD [%] | drill | frog | pig | duck | ext. | mult. |
|---|---|---|---|---|---|---|
| 0°, 10 | 84 | 67 | 48 | 58 | 15 | 17 |
| 0°, 20 | 93 | 78 | 73 | 90 | 22 | 28 |
| 30°, 10 | 77 | 76 | 49 | 86 | 63 | 72 |
| 30°, 20 | 96 | 93 | 77 | 90 | 83 | 91 |
| 60°, 10 | 67 | 63 | 61 | 83 | 65 | 73 |
| 60°, 20 | 94 | 78 | 87 | 87 | 90 | 99 |
| 90°, 10 | 50 | 35 | 42 | 91 | 80 | 87 |
| 90°, 20 | 75 | 53 | 71 | 99 | 98 | 100 |
| Av., 10 | 69 | 60 | 50 | 79 | 56 | 62 |
| Av., 20 | 89 | 75 | 77 | 91 | 73 | 80 |

achieved for 0° camera view. In discussed camera view the pose tracking was done using side-view images of the objects.

Figure 6 depicts rotation errors over time on real images, which have been obtained by the PF-PSO with neural network estimating 2D location of fiducial points and the PnP algorithm. As we can observe, the largest errors were obtained for the extension, which is symmetric and texture-less object. Somewhat larger errors were observed for 30° camera view.

In order to segment the House and Ironman objects we trained a single U-Net on 660 images from the OPT benchmark. A single U-Net has been trained on 1800 images in order to segment all six objects from our dataset. The Dice scores were higher than 95% for all objects. The neural networks for estimation of positions of keypoints were trained on 300 images and evaluated on 50 images.

The complete system for 6D pose estimation has been implemented in Python and Keras framework. On the basis of keypoint positions the object poses were calculated using solvePnPRansac (Lepetit et al., 2009) from OpenCV library. The system runs on an ordinary PC with a CPU/GPU. On PC equipped with i5-8300H CPU 2.30 GHz the segmentation time using U-Net is about 0.3 sec., whereas the 6D pose is estimated in about 0.03 sec. About ten times shortening of time has been observed on TitanX graphics card. Initial experiments conducted with Franka-Emika robot, which has been equipped with Xtion RGB-D sensor demonstrated usefulness of the proposed approach to estimation of 6D pose of objects held in hand. The images for training and evaluating the segmentation algorithm as well as extracted objects with corresponding ground-truth for evaluating the 6D object pose tracking are freely available for download at: http://home.agh.edu.pl/~bkw/src/pose6d.

Table 4: Tracking scores [%] achieved by our algorithm with and without PnP.

| tracking score [%] | 0°, ADD 10% | 0°, ADD 20% | 30°, ADD 10% | 30°, ADD 20% | 60°, ADD 10% | 60°, ADD 20% | 90°, ADD 10% | 90°, ADD 20% | Avg., ADD 10% | Avg, ADD 20% |
|---|---|---|---|---|---|---|---|---|---|---|
| drill w/o PnP | 79 | 88 | 60 | 86 | 54 | 74 | 31 | 59 | 56 | 77 |
| drill with PnP | 84 | 93 | 77 | 96 | 67 | 94 | 50 | 75 | 69 | 89 |
| frog w/o PnP | 31 | 33 | 33 | 37 | 37 | 49 | 12 | 24 | 28 | 36 |
| frog with PnP | 67 | 78 | 76 | 93 | 63 | 78 | 35 | 53 | 60 | 75 |
| pig w/o PnP | 50 | 63 | 44 | 49 | 51 | 59 | 48 | 52 | 48 | 56 |
| pig with PnP | 48 | 73 | 49 | 77 | 61 | 87 | 85 | 88 | 61 | 81 |
| duck w/o PnP | 41 | 71 | 76 | 79 | 61 | 78 | 82 | 100 | 65 | 82 |
| duck with PnP | 58 | 90 | 86 | 90 | 83 | 87 | 91 | 99 | 79 | 91 |
| ext. w/o PnP | 18 | 33 | 55 | 82 | 52 | 73 | 70 | 100 | 49 | 72 |
| ext. with PnP | 15 | 22 | 63 | 83 | 65 | 90 | 80 | 98 | 56 | 73 |
| mult. w/o PnP | 1 | 7 | 61 | 93 | 67 | 96 | 77 | 88 | 51 | 71 |
| mult. with PnP | 17 | 28 | 72 | 91 | 73 | 99 | 87 | 100 | 62 | 80 |
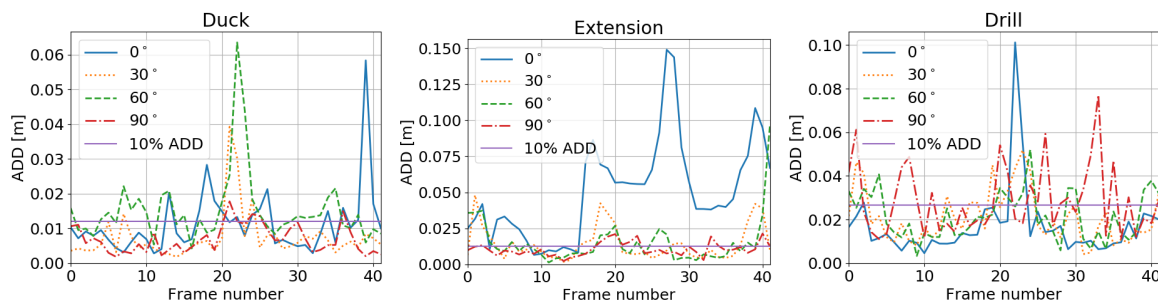


Figure 5: ADD scores over time for images from sequence #2, obtained by PF-PSO and neural network estimating 2D location of fiducial points and PnP algorithm (plots best viewed in color).
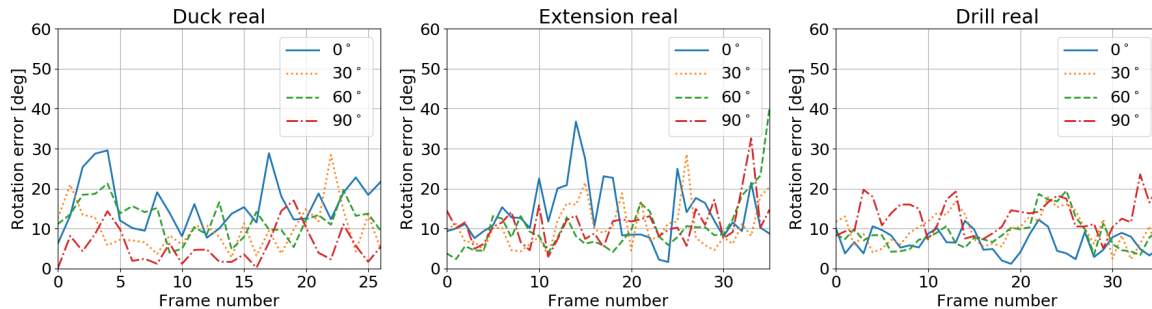


Figure 6: Rotation errors over time for real images, obtained by PF-PSO using poses that were obtained by the PnP algorithm.

# 6 CONCLUSIONS

In this paper, a framework for tracking 6D pose of the object in a sequence of RGB images has been proposed. In this segmentation-driven approach the object of interest is delineated by a single U-net neural network, trained to segment a set of considered objects. A basic PF-PSO algorithm has been evaluated on freely available OPT benchmark dataset for tracking 6D pose of objects. Promising results were obtained on discussed dataset. This basic algorithm has been extended by including in the probability distribution maintained by the PF-PSO a hypothesis about 6D object pose. Such a hypothesis about the object pose is calculated on the basis of object keypoints and the PnP algorithm. The location of fiducial keypoints on images is determined by a neural network, trained separately for each object. The evaluations were done on our dataset that contains both real and synthesized images of six texture-less objects and has been recorded to perform tracking of 6D object pose on RGB images. A separate neural network has been trained to segment all considered objects. Thanks to 3D location of fiducial points on synthetic objects and 2D location of such points on real images, various keypoint-based deep neural network can be trained for object pose estimation in end-to-end framework.

# ACKNOWLEDGEMENTS

# REFERENCES

Arthur, D. and Vassilvitskii, S. (2007). K-means++: The Advantages of Careful Seeding. In *Proc. ACM-SIAM Symp. on Discrete Algorithms*, pages 1027–1035.

Blender Online Community (2020). *Blender - a 3D modelling and rendering package*. Blender Foundation, Stichting Blender Foundation, Amsterdam.

Brachmann, E., Krull, A., Michel, F., Gumhold, S., Shotton, J., and Rother, C. (2014). Learning 6D object pose estimation using 3D object coordinates. In *ECCV*, pages 536–551. Springer.

Brachmann, E., Michel, F., Krull, A., Yang, M., Gumhold, S., and Rother, C. (2016). Uncertainty-driven 6D pose estimation of objects and scenes from a single RGB image. In *CVPR*, pages 3364–3372.

Bradski, G. and Kaehler, A. (2013). *Learning OpenCV: Computer Vision in C++ with the OpenCV Library*. O'Reilly Media, Inc., 2nd edition.

Bugaev, B., Kryshchenko, A., and Belov, R. (2018). Combining 3D model contour energy and keypoints for object tracking. In *ECCV*, pages 55–70, Cham. Springer.

Deng, X., Mousavian, A., Xiang, Y., Xia, F., Bretl, T., and Fox, D. (2019). PoseRBPF: A Rao-Blackwellized Particle Filter for 6D Object Pose Tracking. In *Robotics: Science and Systems (RSS)*.

Fischler, M. A. and Bolles, R. C. (1981). Random Sample Consensus: A Paradigm for Model Fitting with Applications to Image Analysis and Automated Cartography. *Commun. ACM*, 24(6):381–395.

Garrido-Jurado, S., Munoz-Salinas, R., Madrid-Cuevas, F. J., and Marn-Jimenez, M. J. (2014). Automatic generation and detection of highly reliable fiducial markers under occlusion. *Pattern Rec.*, 47(6):2280 – 2292.

He, K., Gkioxari, G., Dollar, P., and Girshick, R. (2017). Mask R-CNN. In *IEEE Int. Conf. on Computer Vision (ICCV)*, pages 2980–2988.

Hinterstoisser, S., Lepetit, V., Ilic, S., Holzer, S., Bradski, G., Konolige, K., and Navab, N. (2013). Model based training, detection and pose estimation of texture-less 3D objects in heavily cluttered scenes. In *Computer Vision – ACCV 2012*, pages 548–562. Springer.

Hodan, T., Haluza, P., Obdrzalek, S., Matas, J., Lourakis, M., and Zabulis, X. (2017). T-LESS: An RGB-D dataset for 6D pose estimation of texture-less objects. In *WACV*, pages 880–888.

Ioffe, S. and Szegedy, C. (2015). Batch Normalization: Accelerating deep network training by reducing internal covariate shift. In *ICML - vol. 37*, pages 448–456.

Kaskman, R., Zakharov, S., Shugurov, I., and Ilic, S. (2019). HomebrewedDB: RGB-D dataset for 6D pose estimation of 3D objects. In *IEEE Int. Conf. on Computer Vision Workshop (ICCVW)*, pages 2767–2776.

Kehl, W., Manhardt, F., Tombari, F., Ilic, S., and Navab, N. (2017). SSD-6D: Making RGB-Based 3D Detection and 6D Pose Estimation Great Again. In *IEEE Int. Conf. on Computer Vision*, pages 1530–1538.

Lepetit, V., Moreno-Noguer, F., and Fua, P. (2009). EPnP: An accurate O(n) solution to the PnP problem. *Int. J. Comput. Vision*, 81(2):155166.

Lepetit, V., Pilet, J., and Fua, P. (2004). Point matching as a classification problem for fast and robust object pose estimation. In *CVPR*, pages 244–250.

Lin, T.-Y., Maire, M., Belongie, S., Hays, J., Perona, P., Ramanan, D., Dollar, P., and Zitnick, C. L. (2014). Microsoft COCO: Common Objects in Context. In *ECCV*, pages 740–755. Springer.

Lopatin, V. and Kwolek, B. (2020). 6D pose estimation of texture-less objects on RGB images using CNNs. In *The 19th Int. Conf. on Artificial Intelligence and Soft Computing*, pages 180–192. Springer.

Majcher, M. and Kwolek, B. (2020). 3D Model-Based 6D Object Pose Tracking on RGB Images Using Particle Filtering and Heuristic Optimization. In *15th Int. The Int. Conf. on Computer Vision Theory and Applications (VISAPP)*, pages 690–697, vol. 5. SciTePress.

Marchand, E., Uchiyama, H., and Spindler, F. (2016). Pose estimation for augmented reality: A hands-on survey. *IEEE Trans. on Vis. and Comp. Graphics*, 22(12):2633–2651.

Peng, S., Liu, Y., Huang, Q., Zhou, X., and Bao, H. (2019). PVNet: Pixel-Wise Voting Network for 6DoF Pose Estimation. In *IEEE Conf. on Comp. Vision and Patt. Rec.*, pages 4556–4565.

Prisacariu, V. A. and Reid, I. D. (2012). PWP3D: Real-Time Segmentation and Tracking of 3D Objects. *Int. J. Comput. Vision*, 98(3):335–354.

Rad, M. and Lepetit, V. (2017). BB8: A scalable, accurate, robust to partial occlusion method for predicting the 3D poses of challenging objects without using depth. In *IEEE Int. Conf. on Comp. Vision*, pages 3848–3856.

Ronneberger, O., Fischer, P., and Brox, T. (2015). U-Net: Convolutional networks for biomedical image segmentation. In *MICCAI*, pages 234–241. Springer.

Vidal, J., Lin, C., and Mart, R. (2018). 6D pose estimation using an improved method based on point pair features. In *Int. Conf. on Control, Automation and Robotics*, pages 405–409.

Whelan, T., Salas-Moreno, R. F., Glocker, B., Davison, A. J., and Leutenegger, S. (2016). ElasticFusion. *Int. J. Rob. Res.*, 35(14):1697–1716.

Wu, P., Lee, Y., Tseng, H., Ho, H., Yang, M., and Chien, S. (2017). A benchmark dataset for 6DoF object pose tracking. In *IEEE Int. Symp. on Mixed and Aug. Reality*, pages 186–191.

Xiang, Y., Schmidt, T., Narayanan, V., and Fox, D. (2018). PoseCNN: A Convolutional Neural Network for 6D Object Pose Estimation in Cluttered Scenes. In *IEEE/RSJ Int. Conf. on Intel. Robots and Systems*.

Zhao, Z., Peng, G., Wang, H., Fang, H., Li, C., and Lu, C. (2018). Estimating 6D pose from localizing designated surface keypoints. *ArXiv*, abs/1812.01387.